GHGT-11

Characterizing small-scale migration behavior of sequestered CO_2 in a realistic geologic fabric

Priya Ravi Ganesh[a]*, Steven L Bryant[a] and Timothy A Meckel[b]

[a]Department of Petroleum and Geosystems Engineering, University of Texas at Austin, 200 E.Dean Keeton Stop C0300, Austin, TX 78712-15851, United States of America
[b]Bureau of Economic Geology, University of Texas at Austin, University Station, Box X, Austin, TX 78713, United States of America

Abstract

For typical field conditions, buoyancy and capillary forces grow dominant over viscous forces within a few hundred meters of the injection wells resulting in remarkably different fluid migration patterns. Reservoir heterogeneity and fluid properties are principal factors influencing CO_2 migration pathways in the buoyancy/capillarity regime. We study the effect of small-scale heterogeneity on buoyant migration of CO_2 in this regime. Capillary channel flow patterns emerge in this regime, as characterized by invasion-percolation simulations in a real meter-scale 2D geologic domain in which sedimentologic heterogeneity has been resolved at sub-millimeter resolution. As the degree of heterogeneity increased in synthetic media, CO_2 migration patterns exhibited a spectrum of structures, from 'dispersed' capillary fingers with minimal rock contact to back-filled 'compact' distributions of saturation with much larger storage efficiency.

1. Introduction

When CO_2 is injected into a storage reservoir during sequestration, viscous forces dominate flow behaviour near the wellbore due to high injection rates and large pressure gradients (regime (a), Figure 1). CO_2 moves in a compact front, completely flooding all the pores it encounters in the rock. The shape of the saturation front in this near-wellbore region is determined by the spatial correlation of permeability in the storage formation [1]. As CO_2 advances into the medium farther from the injection well, the velocity of propagation of CO_2 and the pressure gradient decrease until a point where the pressure gradient from

* Corresponding author. Tel.: +1-512-803-4918; fax: +1 512 471 9605.
E-mail address: priyatrg@utexas.edu, priyatrg@gmail.com.

injection becomes negligible compared to buoyancy forces. At this point (from time t_2 in Figure 1) capillary forces begin to determine whether the meniscus between migrating CO_2 and native brine will move into a pore throat. The capillary pressure of the leading edge of the CO_2 front P_c depends on the height of the connected column of CO_2 from that edge, given by

$$P_c = \Delta \rho g h_{eff}$$ ... (1)

Nomenclature

P_{th}	threshold pressure, capillary entry pressure (porous medium property)
$<P_{th}>$	mean threshold pressure of the medium
σP_{th}	standard deviation, σ of threshold pressure distribution of the medium
P_c	capillary pressure of the leading edge of the CO_2 front
$\Delta \rho$	density difference between CO_2 and native brine
g	acceleration due to gravity
h_{eff}	effective height of the plume front measured vertically from the leading edge to the bottom of continuous column of migrating CO_2
D_mm	grain diameter in mm
IFT	interfacial tension
% domain invaded by CO_2	ratio of number of cells in the domain in which CO_2 is present to the total number of cells in the domain

Generically three possible outcomes exist for this competition between the capillary pressure at the leading edge of the CO_2 plume and the threshold pressure distribution of the reservoir rock [4,5], yielding flow regimes (a), (b) and (c) in Figure 1. In flow regime (a), $P_c > \max(P_{th})$, i.e. the capillary pressure exceeds the maximum threshold pressure of the reservoir rock and *compact flow* of CO_2 occurs where CO_2 enters all pore throats. This would typically be a continuation of the near-wellbore (pressure-gradient driven) migration regime. In flow regime (b) $\min(P_{th}) < P_c < \max(P_{th})$, i.e. the CO_2 capillary pressure is greater than the smallest threshold pressure but does not exceed the highest threshold pressure in that portion of the reservoir rock. The CO_2 migration pattern adopts a *capillary channel* structure characteristic of invasion percolation that is vertically biased due to buoyancy. Because CO_2 migrates through much less of the rock volume, a given mass will migrate much farther in this regime than in compact flow, with important consequence for CO_2 storage [6-9]. In flow regime (c) where the capillary pressure is smaller than the minimum threshold pressure of a *seal rock*, i.e. $P_c < \min(P_{th}^{seal})$, further migration of the plume is blocked or redirected. If CO_2 cannot migrate around this barrier, it will accumulate with progressively increasing P_c similar to natural reservoirs of hydrocarbon or CO_2.

In this paper we present simulations of CO_2 migration for the capillary channel flow regime (regime (b) in Figure 1) for various rocks. We assume that this rock is far from seal rocks and part of a laterally continuous reservoir section (no edge effects; periodic lateral flow boundaries). We quantify effective rock-fluid contact as this CO_2 migrates upward. We treat the limiting case in which a compact plume has just reached the point of transition to buoyancy-dominated migration. Thus a line source (in 2D simulations) of CO_2 is placed at the bottom of the rock section under study. The height of the compact plume is not specified but is by definition sufficient for CO_2 to enter the domain. Thus in the simulator, P_c is initialised with the minimum threshold pressure of the region contacted by the source. Though not modelled explicitly, the column height of the source plume is assumed to build so that CO_2 invades more and more of the domain. Percolation is said to occur once CO_2 traverses the entire height of the model

domain and reaches the top boundary. At percolation the overall CO_2 saturation stops increasing, although flow continues through the media.

We use the commercial software Permedia®, a modified invasion percolation based simulator distributed by Halliburton, to investigate the buoyant rise of CO_2. The simulated behaviour is very similar to results of full-physics simulations with commercial codes such as GEM® when capillarity heterogeneity is explicitly included [10]. One advantage of the IP simulator is that models with large numbers of cells (highly resolved) can be simulated quickly, which typically take much longer using traditional simulators. The basic physics of buoyant migration of the non-wetting CO_2 phase through a heterogeneous domain is an extension of invasion percolation. The key rule governing invasion percolation at the pore scale is that if the capillary pressure (P_c) exceeds the threshold pressure of the pore throat (P_{th}), then nonwetting fluid passes through the throat and enters the adjoining pore; otherwise the pore throat continues to act as a flow barrier. Here we employ the extension of this concept to flows at larger scales, which simply replaces the pore throat with a volume of rock with a characteristic value of capillary entry pressure.
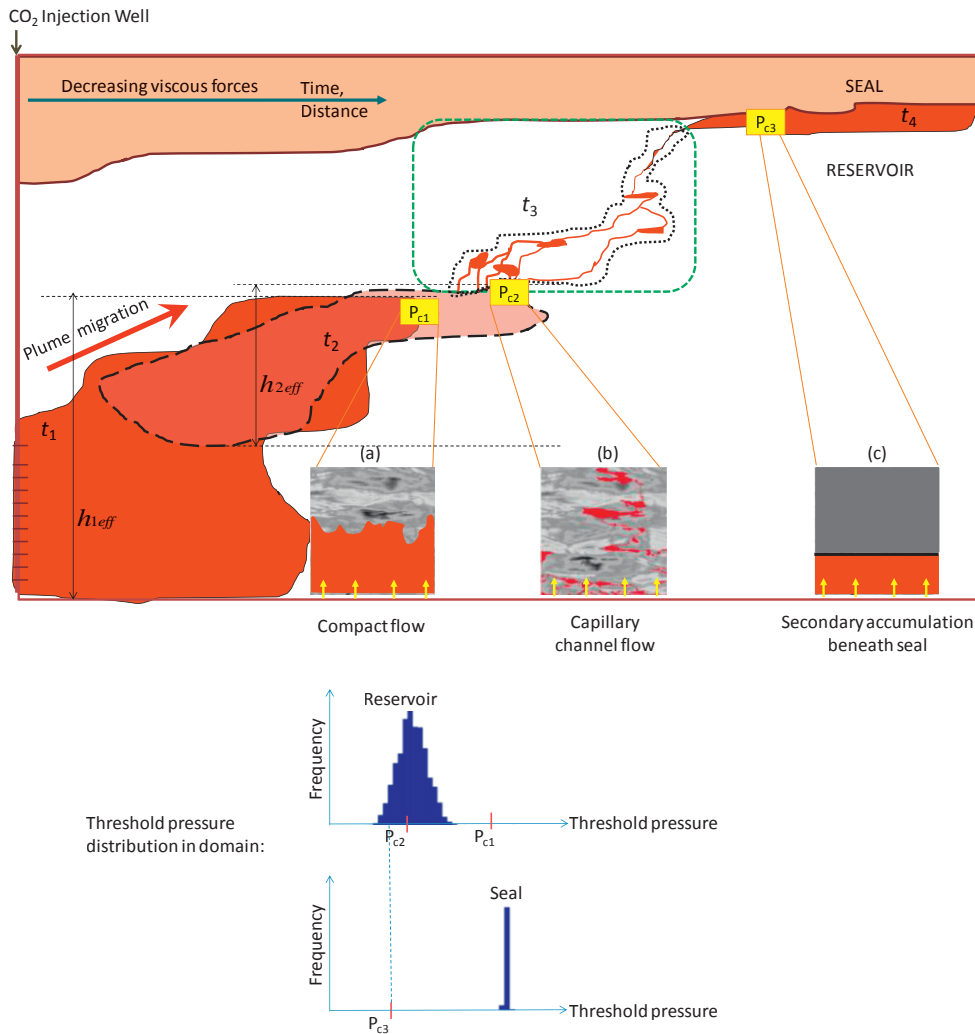
Figure 1: Schematic of spatial and temporal evolution of CO_2 flow regimes from viscous-dominated to buoyancy/capillarity-dominated. The storage reservoir is heterogeneous with a threshold pressure field P_{th} with frequency distribution shown at the bottom of the diagram; the sealing formation has a much larger threshold pressure. h_{eff} is the effective height of the plume front measured vertically from the leading edge to the bottom of continuous column of migrating CO_2. At time t_1, for a continuous column height of h_{1eff} the capillary pressure at the leading edge of the CO_2 plume is $P_{c1} = \Delta\rho g h_{1eff}$. As the CO_2 plume moves through time (outlines of plume at times t_1 through t_4 are shown as black solid or broken lines) and distance in the storage reservoir (extreme vertical exaggeration), possible flow regimes are: (a) *compact flow* where $P_{c1} > \max(P_{th})$; (b) *capillary channel flow* where $\min(P_{th}) < P_{c2} < \max(P_{th})$; and (c) *secondary accumulation beneath a seal* where $P_{c3} < \min(P_{th}^{seal})$. The yellow arrows in the insets describing the flow regimes indicate the CO_2 being sourced from the bottom of the rock section. In this paper, we explore flow regime (b) within the green dotted rectangle.

2. Heterogeneous geologic domain

An important control on plume behaviour in the capillary channel regime is the structure of the heterogeneity in the reservoir. Here we investigate this effect at the small scale (< 1 m) using a highly resolved natural model domain. The domain is a digital representation of a physical geologic specimen. The specimen (Figure 2(a)) is a vertically-oriented, quasi-2D sedimentary relief peel sample (1.0 m × 0.5 m) extracted from the upper portions of a modern point bar of the Brazos River, Texas [11, 12]. The peel broadly consists of cm-scale ripple-laminated well-sorted lower-fine to lower-very-fine sand. Topographic relief of the sample surface reflects varying extent of imbibition of viscous fluid (epoxy) used for sample preparation and thus correlates with key petrophysical properties [13].
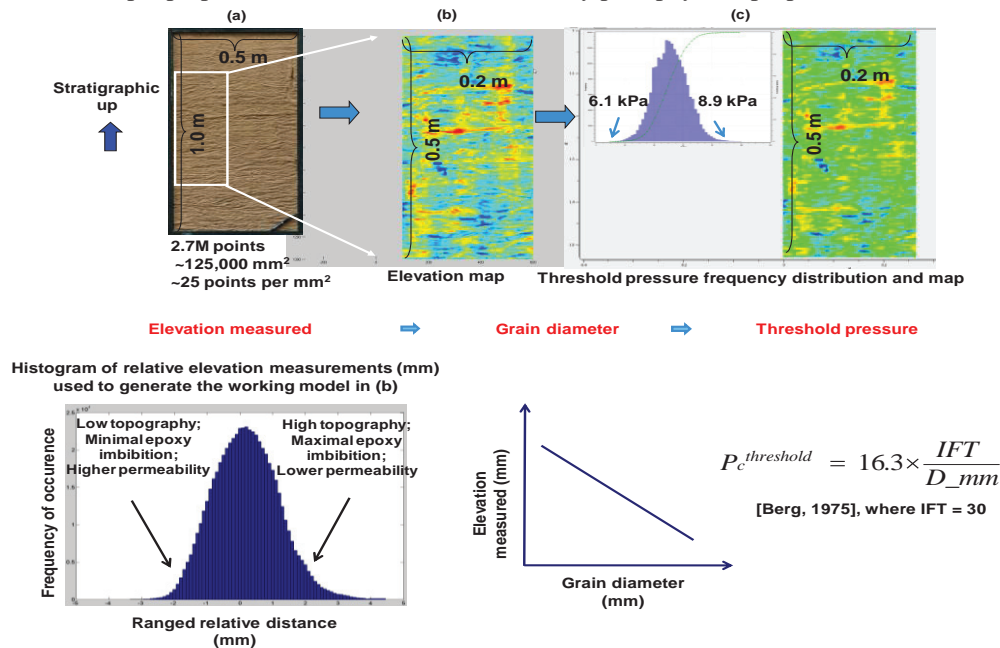

Figure 2: Summary of the geologic model [15]. Optically ranged topography and grain diameter measurements on a 1 m by 0.5 m relief-peel from a river alluvium are used to build high-resolution digital model populated with threshold pressure values. Sequential stages of building the digital model are: (a) Peel specimen subjected to high-resolution laser scanning and imaging techniques to study epoxy imbibition and grain size distribution; (b) Digital elevation map derived from topographical variations in the peel due to epoxy imbibition; (c) Digital high-resolution model (>2 million cells) representing the threshold pressure distribution of the model domain generated from grain diameter measurements corresponding to determined topography.

The high-resolution digital elevation map obtained through laser range scanning (Figure 2(b)) indicates that peel topography is linearly correlated with variations in measured grain size (in mm) and sorting [15]. Higher elevations correspond with greater imbibitions due to smaller average grain size (hotter colours in Figure 2(b) and lighter gray background shades in subsequent simulation results) and lower elevations correspond with lesser imbibition as a result of larger average grain size (cooler colours in Figure 2(b) and darker gray background shades in simulation results). We use this normally-distributed elevation data as a proxy for rock property of interest here, namely, threshold entry pressure for drainage (invasion of CO_2). Values of threshold pressure calculated from the measured grain size distribution were assigned to grid elements by assuming the simple Berg equation [14] applies for CO_2-H_2O system.

$$P_c^{threshold} = P_{th} = 16.3 \times \frac{IFT}{D\_mm} \qquad \text{... (2)}$$

where 16.3 is a constant factor incorporating units conversion, *IFT* is interfacial tension (30 mN/m) for CO_2- H_2O system, *D_mm* is grain diameter in mm, and P_{th} is threshold pressure in kPa.

3. Results and discussion

First we simulate capillary channel flow of CO_2 in the digital model of the whole peel specimen. Then we investigate fundamental geologic drivers influencing CO_2 migration patterns in the medium for various rock properties.

3.1 Simulation of capillary channel flow in the peel specimen

In this section we simulate buoyancy-driven migration of CO_2 in the peel model for the capillary channel migration regime (Figure 3). Maximum and minimum P_{th} values of 6.1 to 8.9 kPa ($<P_{th}>$ = 7.4 kPa) are assigned to the model corresponding to the minimum and maximum grain sizes of 0.055 and 0.08 mm determined for the specimen.
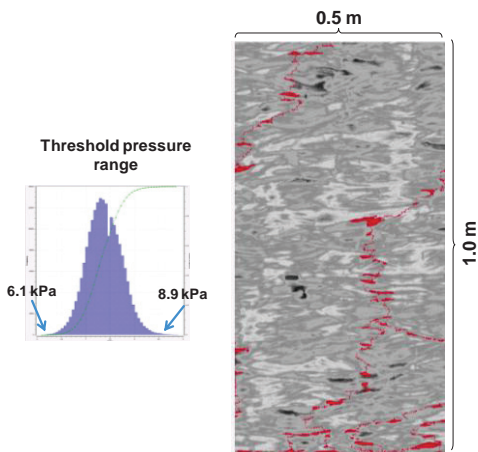

Figure 3: Invasion percolation simulation of CO_2 (red) migrating through the peel model of Fig. 2. Continuous line source was placed at bottom boundary of model domain, left and right boundaries are periodic. The CO_2 flow pattern is characterized as 'fingering' and 2.86% of the model domain is saturated with CO_2 at percolation.

After CO_2 percolates to the top of the domain, no more of the domain will be invaded although flow may continue on the defined pathway. The fraction of the rock volume that contains CO_2 at this point is 2.86%, which is quite small. These capillary channels efficiently transport all CO_2 that enters the domain through a few narrow, generally vertical pathways. The CO_2 occasionally forms small accumulations

below the light gray patches corresponding to barriers having highest threshold pressures in the domain (Figure 3). Simulations that do not account for the spatial variation in capillary entry pressure yield compact displacement fronts with correspondingly much larger CO_2 percentage saturations.

3.2 Effect of heterogeneity on capillary channels

In this section we focus on the capillary channel migration regime in synthetic domains of varying degrees of heterogeneity but with fabric taken from the peel. We vary two aspects of heterogeneity, threshold pressure frequency distribution and the correlation length of the threshold pressures in the horizontal and vertical directions.

One set of simulations are conducted on a randomly chosen 0.4 m × 0.4 m subsection (2000 × 2000 cells) of the peel model to resolve CO_2 migration patterns at native depositional resolution (Figure 4 row A). We vary the standard deviations at 0.02, 0.45 and 1.3 kPa about the mean threshold pressure for each depositional fabric (Figure 4 columns 1, 2 and 3). The mean threshold pressure is set to 7.4 kPa (determined from sampling the peel). Wider ranges of threshold pressure imply more heterogeneity, e.g. poorer sorting or wider grain size distributions, while narrower threshold pressure ranges suggest more homogeneous or well-sorted domains. Analogous simulations are then conducted on two different background depositional fabrics. These fabrics are geostatistical realizations with the ratio of correlation lengths of threshold pressure in the horizontal to vertical direction as 1 and 10 (Figure 4 rows B and C respectively). In each geostatistical model, the correlation length of the threshold pressure in the horizontal direction is held fixed (= 100 × cell height).The rows A, B and C in Figure 4 correspond to varying depositional fabric while the columns 1, 2 and 3 correspond to specific grain size distributions.
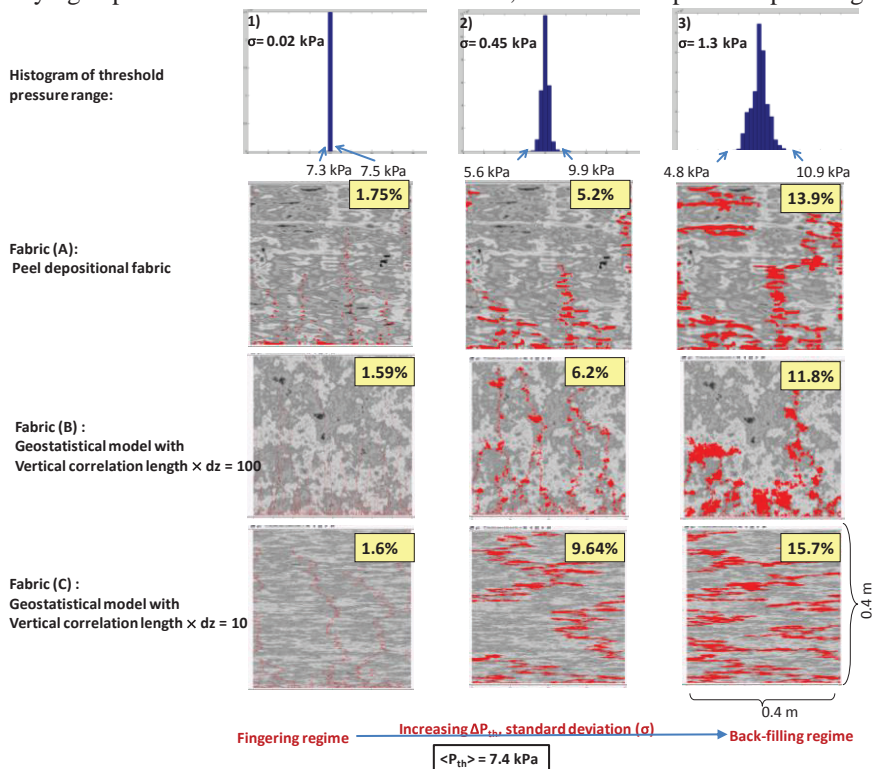

Figure 4: Capillary-channel regime of CO_2 migration. Rows represent a specific depositional fabric while columns represent a specific grain size distribution. The insets at the top-right corner of the realizations indicate the percentage

domain invaded by CO_2 at percolation. Row (A) uses the peel natural depositional fabric. Rows (B) and (C) are geostatistical realizations with prescribed correlation of P_{th} in horizontal and vertical directions. Horizontal correlation length is constant (=$100 \times dz$; $dz = 2$ mm), and vertical correlation length varies by row as indicated. In the panels of each row (A, B, C), the pattern of rising CO_2 transitions from fingering (1st column) to back-filling (3rd column) patterns as the variance in threshold pressure $\sigma(P_{th})$ increases for a fixed depositional fabric. $<P_{th}>$ is 7.4 kPa for all panels. Domains with wider grain size frequency distribution cause CO_2 to back-fill beneath contiguous regions of larger threshold pressure (light gray areas in background P_{th} map) causing CO_2 to invade more of the domain. The influence of the background depositional fabric on capillary channel flow patterns is apparent in panels of the 2nd column. The domains are 2000 cells wide × 2000 cells tall (i.e. 0.4 m × 0.4 m). Density difference between the CO_2 and native brine = 300 kg/m^3 in all cases.

For each depositional fabric (Figure 4 rows A, B and C), we observe CO_2 migration patterns ranging from 'dispersed' capillary fingering structures with minimal rock contact toward back-filled structures with bigger accumulations of CO_2 as heterogeneity increases. For media with more correlation length of threshold pressures in the horizontal compared to the vertical direction, the capillary barriers are more laterally extensive too. Hence they impose a substantial horizontal component of migration that enables more fluid-rock contact as well as higher capacity for capillary trapping.

The fraction of the domain invaded at percolation is plotted in Figure 5 against dimensionless threshold pressure in the two geostatistical model fabrics. The invaded fraction decreases as the heterogeneity of the domain decreases. Higher $\sigma(P_{th})$ values (lower $<P_{th}>/\sigma(P_{th})$ values) implies wider grain size distributions which leads to more probable capillary barriers that drive lateral migration compared to very homogeneous rocks. The flow patterns for specific values of the dimensionless threshold pressure are found to be the same for different depositional fabrics, with the slight variations in the percentage saturation values attributed to the influence of the fabric itself. The 0.4 m × 0.4 m section of the real peel sample is also plotted in Figure 5 (blue data point). The peel behaves as expected from the resulting trend in the geostatistical fabrics. This indicates the possibility of predictive ability for expected flow patterns when the threshold pressure distribution of the medium and fluid properties of the system are known.
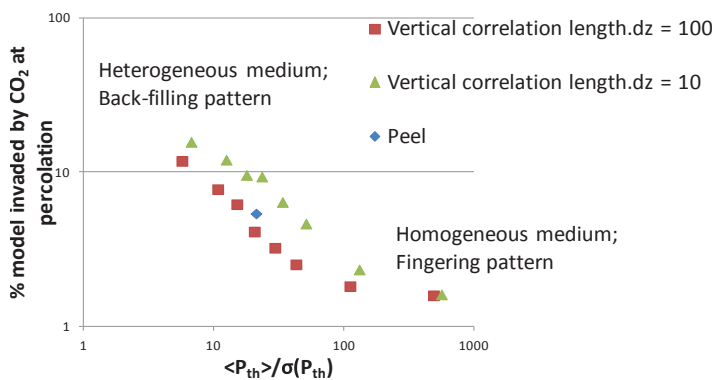

Figure 5: Fraction of rock invaded by CO_2 in capillary-channel regime depends on heterogeneity. Except in very homogeneous domains (large dimensionless threshold pressure), where the invaded fraction approaches a lower bound, a power law relates the invaded fraction (values from Fig. 4) to the dimensionless threshold pressure $<P_{th}>/\sigma(P_{th})$ of the medium for different depositional fabrics. Realizations for line source of CO_2 on the 0.4 m × 0.4 m domain for $<P_{th}> = 7.4$ kPa in two geostatistical models and on the peel are plotted. Each point on the plot represents a realization for a specific threshold pressure distribution on the given depositional fabric. The rocks are more homogeneous for greater values of $<P_{th}>/\sigma(P_{th})$. For the geostatistical models, horizontal correlation length is constant (=$100 \times$ dz; dz = 2 mm), and vertical correlation length varies as vertical correlation × dz = 100 and 10. For a given $<P_{th}> / \sigma(P_{th})$, CO_2 flow patterns in the capillary channel regime are found to be the same.

4. Conclusions

Expected storage efficiency and plume migration behaviour differ greatly in heterogeneous rock wherever viscous forces are negligible compared to buoyancy forces. Buoyancy-dominated plume migration through time and distance in the reservoir falls into three regimes namely, compact flow, capillary channel flow and secondary accumulation beneath a seal. Capillary channel flow regime reduces effective fluid-rock contact compared to compact flow regime. The displacement pattern in capillary channel regime varies between finger-like and back-filling depending on degree of heterogeneity. Fingering pattern is the least efficient in this regime with a storage capacity only a few percent of the nominal value (the pore volume of the rock). In reservoirs with properties conducive to back-filling, namely longer horizontal correlation lengths and wider grain size distributions, rising CO_2 contacts a greater fraction of the reservoir. Accounting for the physics of CO_2 migration under typical storage conditions on a highly resolved meter-scale geological model with mm-scale heterogeneity, we observe a capillary-channel flow regime.

The importance of this work lies in the more accurate treatment of rocks at the micro-scale. This variation in behaviour in the capillary channel flow regime can be captured by standard continuum simulators only when the heterogeneity in the capillary properties of the medium is accounted for at a geologically-representative scale [10, 20 and 21]. Typical coarse-grid simulations that neglect capillarity yield optimistic estimates of the amount of CO_2 held in a region through which a buoyant plume has migrated.

If the peel studied here represented a section of continuous reservoir through which buoyant-dominated migration of CO_2 occurred, then that reservoir would allow CO_2 to finger rapidly and for long distances. Realistic quantification of plume migration patterns helps evaluate the storage potential (amount of CO_2 that can be stored per unit volume of rock) when buoyant migration dominates CO_2 sequestration. This capability can also enable an engineered storage strategy that drives the behaviour toward the desired flow patterns.

Acknowledgements

References

[1] Bryant, S.L., Lakshminarasimhan, S., and Pope, G.A. Buoyancy-dominated multiphase flow and its effect on geological sequestration of CO_2. SPE 2008; J.13 (4): 447-454 SPE-99938-PA.

[2] Kumar, N. CO_2 sequestration: *Understanding the plume dynamics and estimating the risk*. Master's Thesis, Department of Petroleum Engineering, The University of Texas at Austin; 2008.

[3] Auradou H; Maloy, K J; Schmittbuhl, J; Hansen A; Bideau D. Competition between correlated buoyancy and uncorrelated capillary effects during drainage. *Phys. Review E* 1999; 60 (6), 7224-34.

[4] Singh, V; Cavanaugh, A; Hansen, H; Nazarian, B; Iding, M; Ringrose, P. Reservoir modeling of CO_2 plume behavior calibrated against monitoring data from Sleipner, Norway. Paper 134891 presented at the *SPE Annual Technical Conference and Exhibition* held in Florence, Italy, 19-22 September 2010.

[5] Zhang, C; Oostrom, M; Wietsma, T W.; Grate, J W.; Warner, M G., Influence of viscous and capillary forces on immiscible fluid displacement: pore-scale experimental study in a water-wet micromodel demonstrating viscous and capillary fingering. *Energy Fuels* 2010; DOI:10.1021/ef101732k.

[6] Carruthers, D J.F. *Transport modelling of secondary oil migration using gradient-driven invasion percolation techniques*. Ph.D. Dissertation, Department of Petroleum Engineering, Heriot-Watt University, Edinburgh, Scotland UK; 1998.

[7] Krevor, S C.M.; Pini, R; Li, B; Benson, S M. Capillary heterogeneity trapping of CO_2 in a sandstone rock at reservoir conditions. *Geophys. Res. Lett.* 2011; 38, L15401; DOI:10.1029/2011GL048239.

[8] Luo, X.R.; Zhou, B.; Zhao, S.X., Zhang, F.Q; Vasseur, G. Quantitative estimates of oil losses during migration, part I: the saturation of pathways in carrier beds. *Journal of Petroleum Geology* 2007; 30(4), 375-387.

[9] Ringrose, P.S.; Corbett, P.W.M. Controls on two-phase fluid flow in heterogeneous sandstones. Geofluids: Origin, Migration and Evolution of fluids in Sedimentary Basins, *Geol. Soc. Spec. Pub.* 1994; 78, 141-150.

[10] Saadatpoor, E; Bryant, S L.; Sepehrnoori, K. New trapping mechanism in carbon sequestration. *Transp in Porous Media* 2009; 82, 3-17.

[11] Bernard, H.A., and Major, C.F., Jr., Recent meander belt deposits of the Brazos River: An alluvial "sand" model: *AAPG Bull.* 1963; 47(2): 350.

[12] Bernard H.A., Major, C.F., Jr., Parrott, B.S., and Le Blanc, R.J., Sr. Recent sediments of southeast Texas: A field guide to the Brazos alluvial and deltaic plains and the Galveston barrier island complex, Bureau of Economic Geology, The University of Texas at Austin, *Guidebook 11* 1970.

[13] McMullen, R.M. and Allen, J.R.L. Presentation of sedimentary structures in wet unconsolidated sands using polyester resins, *Mar. Geol.* 1964; 1:88-97.

[14] Berg, R.R. Capillary pressures in stratigraphic traps. *AAPG Bull.* 1975; 59(6), 939-956.

[15] Meckel, T.A. Digital rendering of sedimentary-relief peels: implications for clastic facies characterization and fluid flow, 2012; Paper in review.

[16] Glass, R J.; Conrad, S H.; Peplinski, W. Gravity-destabilized nonwetting phase invasion in macroheterogeneous porous media: Experimental observations of invasion dynamics and scale analysis. *Water Resources Research* November 2000; 36(11), Pages 3121-3137.

[17] Cottin, C; Bodiguel, H; Colin, A. Drainage in two-dimensional porous media: From capillary fingering to viscous flow. *Phys. Review E* 2010; 80, 046315; DOI:10.1103/PhyRevE.82.046315.

[18] Ide, S.T; Jessen, K; Orr Jr., F M. Storage of CO_2 in saline aquifers: Effects of gravity, viscous and capillary forces in amount and timing of trapping. *Int. Journal of Greenhouse Gas Control* 2007; 481-491; DOI:10.1016/S1750-5836(07)00091-6.

[19] Salomao, M.C. Analysis of flow in spatially correlated systems by applying the percolation theory. Paper 39039 presented at the fifth *LACPEC* held in Rio de Janeiro, Brazil, 30 August - 3 September 1997.

[20] Luo, X.R.; Yan, J.Z; Zhou, B.; Hou, P; Wang, W.; Vasseur, G. Quantitative estimates of oil losses during migration, part II: measurement of the residual oil saturation in migration pathways. *Journal of Petroleum Geology* 2008; 31(2), 179-190.

[21] Hermanrud, C; Teige, G M G; Iding, M; Eiken, Ola'Rennan, L; Ostmo, S. Differences between flow of injected CO_2 and hydrocarbon migration. *Petroleum Geology Conference series* 2010; 7, 1183-1188; DOI:10.1144/0071183.

[22] Ravi Ganesh, P; *Geologic drivers affecting buoyant plume migration patterns in small-scale heterogeneous media: Characterizing capillary channels of sequestered CO_2*. Master's thesis, Department of Petroleum and Geosystems Engineering, The University of Texas at Austin, December 2012.